
1 **Underestimation of Anthropogenic Organosulfates in Atmospheric**
2 **Aerosols in Urban Regions**

3 *Yanting Qiu¹#, Junrui Wang¹#, Tao Qiu², Jiajie Li³, Yanxin Bai⁴, Teng Liu¹, Ruiqi Man¹,*
4 *Taomou Zong¹, Wenxu Fang¹, Jiawei Yang¹, Yu Xie¹, Zeyu Feng¹, Chenhui Li³, Ying Wei³,*
5 *Kai Bi⁵, Dapeng Liang², Ziqi Gao⁶, Zhijun Wu^{1,*}, Yuchen Wang^{4,*}, Min Hu¹*

6 ¹ State Key Laboratory of Regional Environment and Sustainability, College of
7 Environmental Sciences and Engineering, Peking University, Beijing 100871, China;

8 ² Key Lab of Groundwater Resources and Environment of the Ministry of Education,
9 College of New Energy and Environment, Jilin University, Changchun 130012, China

10 ³ College of Environment and Ecology, Laboratory of Compound Air Pollutants
11 Identification and Control, Taiyuan University of Technology, Taiyuan, 030024, China

12 ⁴ College of Environmental Science and Engineering, Hunan University, Changsha,
13 Hunan, 410082, China

14 ⁵ Beijing Weather Modification Center, Beijing Meteorological Service, Beijing, China

15 ⁶ University of Virginia Environmental Institute, Charlottesville, VA 22902, United States

16 #: Yanting Qiu and Junrui Wang contributed equally to this work

17 *Correspondence Author:

18 Zhijun Wu (zhijunwu@pku.edu.cn) and Yuchen Wang (ywang@hnu.edu.cn)

19

20 **ABSTRACT**

21 Organosulfates (OSs) are important components of organic aerosols, which serve as
22 critical tracers of secondary organic aerosols (SOA). However, molecular composition,
23 precursor-OS correspondence, and formation driving factors of OSs at different
24 atmospheric conditions have not been fully constrained. In this work, we integrated OS
25 molecular composition, precursor-constrained positive matrix factorization (PMF) source
26 apportionment, and OS-precursor correlation analysis to classify OS detected from PM_{2.5}
27 samples according to their volatile organic compounds (VOCs) precursors collected from
28 three different cities (Beijing, Taiyuan, and Changsha) in China. This new approach
29 enables the accurate classification of OSs from molecular perspective. Compared with
30 conventional classification methods, we found the mass fraction of Aliphatic OSs
31 (including nitrooxy OSs; NOSs) increased by 22.0%, 17.8%, and 10.3% in Beijing,
32 Taiyuan, and Changsha, respectively, highlighting the underestimation of Aliphatic OSs
33 in urban regions. The formation driving factors of Aliphatic OSs were further investigated.
34 We found that elevated aerosol liquid water content promoted the formation of Aliphatic
35 OSs only when aerosols transition from non-liquid state to liquid state. In addition,
36 enhanced inorganic sulfate mass concentrations, and O_x (O_x = NO₂ + O₃) concentrations,
37 as well as decreased aerosol pH commonly facilitated the formation of Aliphatic OSs.
38 These results reveal a significant underestimation of OSs derived from anthropogenic
39 emissions, particularly Aliphatic OSs, highlighting the need for a deeper understanding
40 of SOA formation and composition in urban environments.

41 **KEY WORDS:** organosulfate; non-target analysis; high-resolution mass spectrometry;
42 secondary organic aerosol; PMF source apportionment

43

44 1. Introduction

45 Due to the diversity of natural and anthropogenic emissions and the complexity of atmospheric
46 chemistry, investigating the chemical characterization and formation mechanisms of secondary
47 organic aerosols (SOA) remains challenging. Among SOA components, organosulfates (OSs) have
48 emerged as key tracers (Brüggemann et al., 2020; Hoyle et al., 2011), as their formation is primarily
49 governed by secondary atmospheric processes. Moreover, OS significantly influence the aerosol
50 physicochemical properties, including acidity (Riva et al., 2019; Zhang et al., 2019), hygroscopicity
51 (Estillore et al., 2016; Ohno et al., 2022; Hansen et al., 2015), and light-absorption properties (Fleming
52 et al., 2019; Jiang et al., 2025). Therefore, a deeper understanding of OS abundance, sources, and
53 formation drivers is crucial for elucidating SOA formation and its properties.

54 Quantifying OS abundance is critical to assess their contribution to SOA. However, this is
55 difficult due to the large number and structural diversity of OSs molecules and the lack of authentic
56 standards. Most studies quantify a few representative OSs using synthetic or surrogate standards
57 (Wang et al., 2020; Wang et al., 2017; Huang et al., 2018b; He et al., 2022), while non-target analysis
58 (NTA) with high-resolution mass spectrometry (HRMS) offers broader molecular characterization
59 (Huang et al., 2023a; Wang et al., 2022b; Cai et al., 2020). Although NTA combined with surrogate
60 standards allows molecular-level (semi-)quantification, overall OS mass concentration remain
61 underestimated, and many OSs remain unidentified (Lukács et al., 2009; Cao et al., 2017; Tolocka and
62 Turpin, 2012; Ma et al., 2025).

63 Classifying OS based on their precursors is a powerful approach for understanding OS formation
64 from a mechanistic perspective. OSs from specific precursors generally share similar elemental
65 compositions, with characteristic ranges of C atoms, double bond equivalents (DBE), and aromaticity
66 equivalents (Xc). For example, isoprene-derived OSs typically contain 4–5 C atoms; monoterpene-
67 and sesquiterpene-derived OSs usually have 9–10 and 14–15 C atoms, respectively (Lin et al., 2012;
68 Riva et al., 2016c; Wang et al., 2019a; Surratt et al., 2008; Riva et al., 2015). An “OS precursor map,”
69 correlating molecular weight and carbon number based on chamber studies, has been developed to
70 classify OSs accordingly (Wang et al., 2019a). However, these approaches often oversimplify OS
71 formation by relying solely on elemental composition, leaving many OSs without identified precursors.

72 The formation mechanisms of OS remain incompletely understood, though several driving
73 factors have been identified through controlled chamber experiments and ambient observations. For
74 instance, increased aerosol liquid water content (ALWC) enhances OS formation by promoting the
75 uptake of gaseous precursors (Xu et al., 2021a; Wang et al., 2021b). Inorganic sulfate can also affect
76 OS formation by acting as nucleophiles via epoxide pathway (Eddingsaas et al., 2010; Wang et al.,
77 2020). However, meteorological conditions vary across cities, meaning the relative importance of
78 these factors may differ by location. Thus, evaluating these formation drivers under diverse
79 atmospheric conditions is essential. Identifying both common and region-specific drivers is key to a
80 comprehensive understanding of OS formation mechanisms.

81 In this study, we employed NTA using ultra-high performance liquid chromatography (UHPLC)
82 coupled with high-resolution mass spectrometry (HRMS) to characterize OS molecular composition
83 in PM_{2.5} samples from three cities. Identified OSs were classified by their VOCs precursors, including

84 aromatic, aliphatic, monoterpene, and sesquiterpene VOCs, via precursor-constrained positive matrix
85 factorization (PMF). Mass concentrations were quantified or semi-quantified using authentic or
86 surrogate standards. Additionally, spatial variations in OS concentrations and co-located
87 environmental factors were analyzed to distinguish both common and site-specific drivers of OS
88 formation.

89 **2. Methodology**

90 **2.1 Sampling and Filter Extraction**

91 Field observations were conducted during winter (December 2023 to January 2024) at three urban
92 sites in China: Beijing, Taiyuan, and Changsha. The site selection was based on contrasts in winter
93 meteorological conditions and dominate $\text{PM}_{2.5}$ sources. For meteorological conditions, Beijing and
94 Taiyuan represent northern Chinese cities with cold, dry conditions (low RH). In comparison,
95 Changsha is characterized by relatively higher winter RH. In terms of $\text{PM}_{2.5}$ sources, Taiyuan is a
96 traditional industrial and coal-mining base, Changsha's pollution profile is more influenced by traffic
97 and domestic cooking emissions, whereas Beijing is characterized by a high mass fraction of
98 secondary aerosols. This enables a comparative analysis of OS formation mechanisms under varied
99 atmospheric conditions. In Beijing, $\text{PM}_{2.5}$ samples were collected at the Peking University Atmosphere
100 Environment Monitoring Station (PKUERS; 40.00°N, 116.32°E), as detailed in previous studies
101 (Wang et al., 2023a). Sampling in Taiyuan and Changsha took place on rooftops at the Taoyuan
102 National Control Station for Ambient Air Quality (37.88°N, 112.55°E) and the Hunan Hybrid Rice
103 Research Center (28.20°N, 113.09°E), respectively (see Figure S1).

104 Daily $\text{PM}_{2.5}$ samples were collected on quartz fiber filters ($\phi = 47$ mm, Whatman Inc.) from 9:00
105 to 8:00 local time the next day. All quartz fiber filters were pre-baked at 550 °C before sampling to
106 remove the background organic matters. In Beijing and Taiyuan, RH-resolved sampling was
107 performed using an RH-resolved sampler, stratifying daily samples into low ($\text{RH} \leq 40\%$), moderate
108 ($40\% < \text{RH} \leq 60\%$), and high ($\text{RH} > 60\%$) RH regimes with the sampling flow rate of 38 L/min. Due
109 to persistently high RH in Changsha, a four-channel sampler (TH-16, Wuhan Tianhong Inc.) collected
110 $\text{PM}_{2.5}$ samples without RH stratification with the flow rate of 16.7 L/min. Consequently, Beijing and
111 Taiyuan collected one or more samples daily, whereas Changsha collected one sample per day. A total
112 of 40, 64, and 30 samples were obtained from Beijing, Taiyuan, and Changsha, respectively. The
113 samples were stored in a freezer at -18 °C immediately after collection. The maximum duration
114 between the completion of sampling and the start of chemical analysis was approximately 40 days.
115 Prior to analysis, all samples were equilibrated for 24 hours under controlled temperature (20 ± 1 °C)
116 and RH (40-45%) within a clean bench, in order to allow the filters to reach a stable, reproducible
117 condition for subsequent handling and to minimize moisture condensation. Average daily $\text{PM}_{2.5}$ mass
118 concentrations and RH during sampling are summarized in Table S1.

119 Sample extraction followed established protocols (Wang et al., 2020). Briefly, filters were
120 ultrasonically extracted twice for 20 minutes. A total volume of 10 mL of LC-MS grade methanol
121 (Merck Inc.) was used for each sample. All extracts were filtered through 0.22 μm PTFE syringe filters,
122 and evaporated under a gentle stream of high-purity N_2 (>99.99%). The dried extracts were then

123 redissolved in 2 mL of LC-MS grade methanol for analysis. This step was necessary to achieve
124 sufficient sensitivity for the detection of OSs with low concentration.

125 During the campaign, gaseous pollutants (SO₂, NO₂, O₃, CO) were monitored using automatic
126 analyzers. PM_{2.5} and PM₁₀ mass concentrations were measured by tapered element oscillating
127 microbalance (TEOM). Water-soluble ions (Na⁺, NH₄⁺, K⁺, Mg²⁺, Ca²⁺, Cl⁻, NO₃⁻, SO₄²⁻) were
128 analyzed with the Monitor for AeRosols and Gases in ambient Air (MARGA) coupled with ion
129 chromatography. Organic carbon (OC) and elemental carbon (EC) were quantified by online OC/EC
130 analyzers or carbon aerosol speciation systems. Trace elements in PM_{2.5} were determined by X-ray
131 fluorescence spectrometry (XRF). Additionally, VOCs concentrations were measured using an online
132 gas chromatography-mass spectrometry (GC-MS) system with a one-hour time resolution in Taiyuan
133 and Changsha. Table S2 summarizes the monitoring instruments deployed at each site. All instruments
134 were calibrated to ensure the reliability of the measurement data. Specifically, the online gas pollutants
135 and particulate matter automatic analyzers underwent automatic zero/span checks every 24 hours at
136 0:00 local time. For MARGA-ion chromatography, OC/EC analyzers, and XRF systems were
137 calibrated weekly. The online GC-MS system was automatically calibrated every 24 hours using
138 standard VOCs mixture.

139 2.2 Identification of Organosulfates

140 The molecular composition of PM_{2.5} extracts was analyzed using an ultra-high performance
141 liquid chromatography (UHPLC) system (Thermo Ultimate 3000, Thermo Scientific) coupled with an
142 Orbitrap HRMS (Orbitrap Fusion, Thermo Scientific) equipped with an electrospray ionization (ESI)
143 source operating in negative mode. Chromatographic separation was achieved on a reversed-phase
144 Accucore C18 column (150 × 2.1 mm, 2.6 μm particle size, Thermo Scientific). For tandem MS
145 acquisition, full MS scans (*m/z* 70–700) were collected at a resolving power of 120,000, followed by
146 data-dependent MS/MS (ddMS²) scans (*m/z* 50–500) at 30,000 resolving power. Detailed UHPLC-
147 HRMS² parameters are provided in Text S1.

148 NTA was performed using Compound Discoverer (CD) software (version 3.3, Thermo Scientific)
149 to identify chromatographic peak features (workflow details in Table S3). Molecular formulas were
150 assigned based on elemental combinations C_cH_hO_oN_nS_s (c = 1–90, h = 1–200, o = 0–20, n = 0–1, s =
151 0–1) within a mass tolerance of 0.005 Da with up to one ¹³C isotope. Formulas with hydrogen-to-
152 carbon (H/C) ratios outside 0.3–3.0 and oxygen-to-carbon (O/C) ratios beyond 0–3.0 were excluded
153 to remove implausible assignments. We calculated the double bond equivalent (DBE) and aromatic
154 index represented by X_c based on assigned elemental combinations using eqs. (1) and (2), where *m*
155 and *k* were the fractions of oxygen and sulfur atoms in the π-bond structures of a compound (both *m*
156 and *k* were presumed to be 0.50 in this work (Yassine et al., 2014)).

157
$$\text{DBE} = c - 0.5h + 0.5n + 1 \quad (1)$$

158
$$X_c = (3 \times (\text{DBE} - m \times o - k \times s) - 2) / (\text{DBE} - m \times o - k \times s) \quad (\text{if } \text{DBE} < (m \times o + k \times s) \text{ or } X_c < 0, \text{ then } X_c \text{ was set to } 0) \quad (2)$$

160 In eq. (2), X_c is an important indicator of whether aromatic rings exist in a molecule. Studies
161 have proved that a molecule is considered aromatic if its X_c value exceeds 2.50 (Ma et al., 2022;
162 Yassine et al., 2014). OSs were selected based on compounds with O/S ≥ 4 and HSO₄⁻ (*m/z* 96.96010)

163 fragments were observed in their corresponding MS^2 spectra. Among them, if N number is 1, O/S ≥ 7 ,
164 and their MS^2 spectra showed ONO_2^- (m/z 61.98837) fragment, these OSs were defined as nitrooxy
165 OSs (NOSs). It should be noted that several CHOS (composed of C, H, O, and S atoms, hereinafter)
166 and CHONS species were not determined as OSs due to their low-abundance and insufficient to trigger
167 reliable data-dependent MS^2 acquisition, which may lead to an underestimation of total OS mass
168 concentration.

169 **2.3 Classification and Quantification/Semi-quantification of Organosulfates**

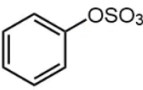
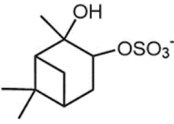
170 To ensure the reliability of quantitative analysis and source attribution, this study focuses on OS
171 species with $C \geq 8$. The exclusion of smaller OSs ($C \leq 7$) is based on challenges in their unambiguous
172 identification, including co-elution with interfering compounds (Liu et al., 2024), and higher
173 uncertainty in precursor assignment due to the lack of characteristic “tracer” molecules in laboratory
174 experiments. Though redisslove using pure methanol may not be the ideal solvent for retaining polar,
175 early-eluting compounds on the reversed-phase column, it provided a consistent solvent for the
176 analysis of the mid- and non-polar OS species ($C \geq 8$) that are the focus of this study.

177 To classify the identified OSs, we employed and compared two distinct classification approaches.
178 Firstly, a conventional classification approach relies primarily on precursor–product relationships
179 established through controlled laboratory chamber experiments and field campaigns (Zhao et al., 2018;
180 Wang et al., 2021a; Deng et al., 2021; Xu et al., 2021b; Mutzel et al., 2015; Brüggemann et al., 2020;
181 Yang et al., 2024; Duporté et al., 2020; Huang et al., 2023b; Wang et al., 2022b; Riva et al., 2016a).
182 Based on these established precursor–product relationships, detected OSs and NOSs were classified
183 into four groups: Monoterpene OSs (including Monoterpene NOSs, hereinafter), Aliphatic OSs
184 (including Aliphatic NOSs, hereinafter), Aromatic OSs (including Aromatic NOSs, hereinafter), and
185 Sesquiterpene OSs (including Sesquiterpene NOSs, hereinafter) (see Table S4 for details). It is
186 apparently that this approach has notable limitations when applied to detected OS in atmospheric
187 aerosols. A substantial fraction of detected OSs does not match known laboratory tracers and are thus
188 labeled Unknown OSs (including Unknown NOSs, hereinafter).

189 Synthetic α -pinene OSs ($C_{10}H_{17}O_5S^-$) and NOSs ($C_{10}H_{16}NO_7S^-$) served for (semi-)quantifying
190 Monoterpene and Sesquiterpene OSs. Their detailed synthesis procedure was described in previous
191 study (Wang et al., 2019b). Potassium phenyl sulfate ($C_6H_5O_4S^-$) and sodium octyl sulfate ($C_8H_{17}O_4S^-$)
192 were used for Aromatic OSs and Aliphatic OSs due to lack of authentic standards (Yang et al., 2023;
193 He et al., 2022; Staudt et al., 2014). Unknown OSs were semi-quantified by surrogates with similar
194 retention times (RT) (Yang et al., 2023; Huang et al., 2023b). Table 1 lists the standards, retention
195 times, and quantified categories. Unknown OSs were absent between 2.00–5.00 min and after 13.60
196 min.

197 **Table 1** Chemical structure, UHPLC retention time, and quantified categories of standards used in
198 the quantification/semi-quantification of OSs and NOSs

| Formula (M-H) | m/z ([M-H] $^-$) | Chemical structure | UHPLC RT (min) | Quantified OSs categories |
|------------------|------------------------|--------------------|-------------------|---------------------------|
|------------------|------------------------|--------------------|-------------------|---------------------------|

| | | | | |
|-----------------------|-----------|---|-------|---|
| $C_6H_5O_4S^-$ | 172.99140 |  | 0.92 | Aromatic OSs, Unknown OSs (RT 0.50-2.00 min) |
| $C_8H_{17}O_4S^-$ | 209.08530 |  | 10.30 | Aliphatic OSs, Unknown OSs (RT 10.00-13.60 min) |
| $C_{10}H_{17}O_5S^-$ | 249.08022 |  | 7.73 | Monoterpene OSs, Sesquiterpene OSs, Unknown OSs (RT 5.00-10.00 min) |
| $C_{10}H_{16}NO_7S^-$ | 294.06530 |  | 9.26 | Monoterpene NOSSs and Sesquiterpene NOSSs |

199 This quantification approach introduces inherent uncertainty, as differences in molecular
 200 structure and functional groups between a surrogate and detected OSs have different ionization
 201 efficiency (Ma et al., 2025), which is a well-documented challenge in NTA of complex mixtures.
 202 However, this approach provides a consistent basis for comparing the relative abundance of OS in
 203 different cities and their formation driving factors. Hence, the mass concentration of detected OSs is
 204 still reliable in understanding their classification and formation driving factors.

205 To classify the Unknown OSs, we first calculated the X_c of each species. Those with $DBE > 2$ and
 206 $X_c > 2.50$ were designated as Aromatic OSs (Yassine et al., 2014). Subsequently, constrained positive
 207 matrix factorization (PMF) analysis was performed using EPA PMF 5.0. The input matrix comprised
 208 the mass concentrations of 60 unclassified OS species across all samples.

209 Figure S2 shows the source profiles of PMF model. Four factors were identified in this study.
 210 Specifically, Factor 1 is identified as Aliphatic OSs due to the dominant contributions from species
 211 like $C_{11}H_{22}O_5S$ and $C_{12}H_{24}O_5S$, which possess low DBE and are characteristic of long-chain alkane
 212 oxidation (Yang et al., 2024). This assignment is strongly supported by the co-variation of this factor
 213 with n-dodecane. Similarly, Factor 2 is classified as Aromatic OSs, highlighted by the significant
 214 contribution of $C_{10}H_{10}O_7S$ and $C_{11}H_{14}O_7S$, which have been proved as OSs derived from typical
 215 aromatic VOCs (Riva et al., 2015). In addition, the high contributions of benzene, toluene, and styrene
 216 in Factor 2 further suggests that this factor should be classified as Aromatic OSs. As for Factor 3 and
 217 Factor 4 is confirmed by the prominence of established Monoterpene OSs (Surratt et al., 2008; Iinuma
 218 et al., 2007) (e.g., $C_{10}H_{18}O_5S$, $C_{10}H_{17}NO_7S$) and Sesquiterpene OSs (Wang et al., 2022b) (e.g.,
 219 $C_{14}H_{28}O_6S$, $C_{15}H_{25}NO_7S$), respectively. Moreover, isoprene showed high contribution in both Factors
 220 3 and 4. As monoterpenes and sesquiterpenes cannot be detected by online GC-MS, considering that
 221 monoterpenes and sesquiterpenes mainly originate from biogenic sources and strongly correlate with
 222 isoprene (Guenther et al., 2006; Sakulyanontvittaya et al., 2008), therefore, isoprene is used as a
 223 surrogate marker as Monoterpene OSs and Sesquiterpene OSs. High contribution of isoprene in
 224 Factors 3 and 4 proved that these factors were respectively determined as Monoterpene OSs and
 225 Sesquiterpene OSs. Based on marker species, Unknown OSs were further categorized into
 226 Monoterpene, Aromatic, Aliphatic, and Sesquiterpene OSs.

227 The model was executed with 10 runs to ensure stability. The ratio of Q_{robust}/Q_{true} for this solution
 228 was stabilized below 1.50, indicating a robust fit without over-factorization. Furthermore, the scaled

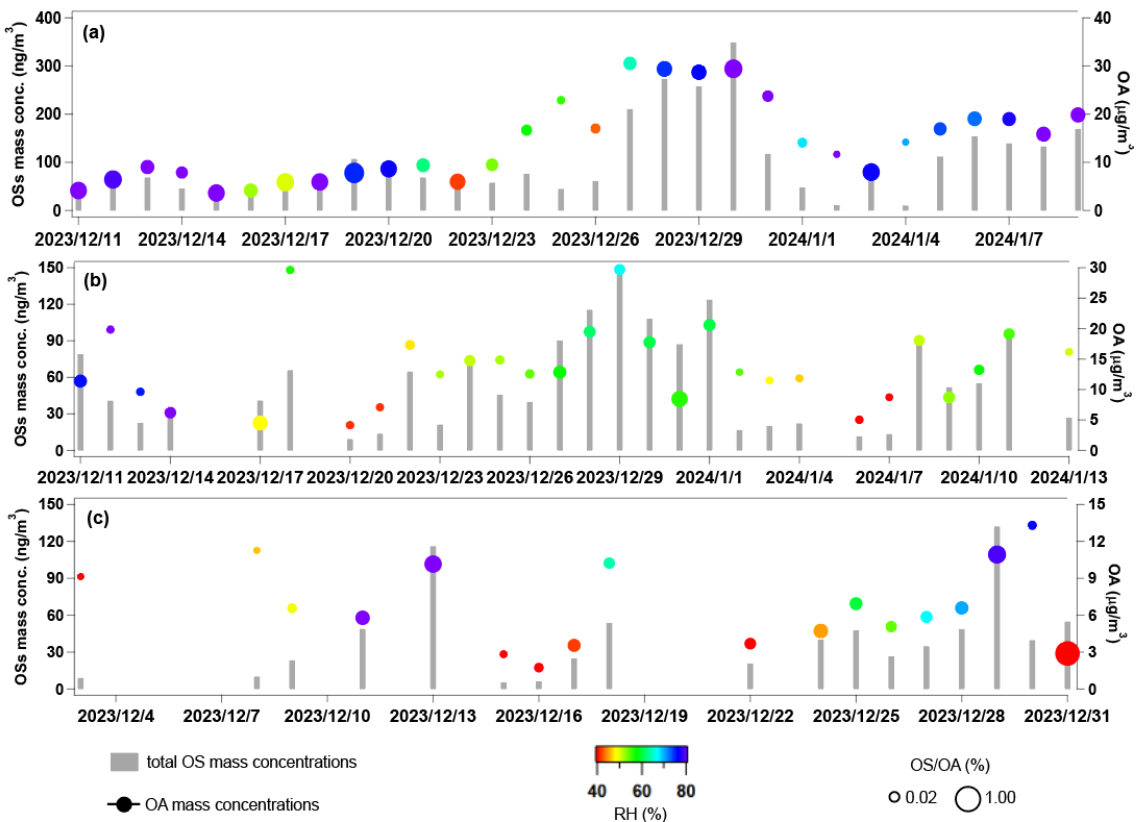
residual matrix (see Figure S3), demonstrating that residuals are randomly distributed and predominantly within the acceptable range of -3 to 3. Correlation coefficients between classified OSs and corresponding VOCs (Monoterpene OSs vs. isoprene; Aromatic OSs vs. benzene; Aliphatic OSs vs. n-dodecane; Sesquiterpene OSs vs. isoprene) were calculated as a statistical auxiliary variable to verify the reliability of PMF results. The arithmetic mean of hourly VOCs within each corresponding filter sampling period was calculated to align the time resolution of VOCs and OS mass concentration. Species with $R < 0.40$ were excluded to avoid potential incorrect classification.

To validate classification accuracy, MS^2 fragment patterns were analyzed (Table S5). Diagnostic fragments supported the assignments: Aliphatic OSs showed sequential alkyl chain cleavages ($\Delta m/z = 14.0157$) and saturated alkyl fragments ($[C_nH_{2n+1}]^-$ or $[C_nH_{2n-1}]^-$); Monoterpene OSs displayed $[C_nH_{2n-3}]^-$ fragments; Aromatic OSs exhibited characteristic aromatic substituent fragments ($[C_6H_5R-H]^-$, R = alkyl, carbonyl, -OH, or H). While absolute certainty for every individual OS in a complex ambient mixture is unattainable, integrating the precursor-constrained PMF model, tracer VOCs correlation analysis, and MS^2 fragment patterns validation significantly reduces the likelihood of systematic misclassification.

3. Results and Discussion

3.1 Concentrations, Compositions, and Classification of Organosulfates

Figure 1 shows the temporal variations of OS and organic aerosols (OA) mass concentrations, as well as RH, during the sampling period across the three cities. The total mass concentration of OS reported in this study is the sum of the (semi-)quantified concentrations of all individual OS species that met the identification criteria described in Section 2.3. The mean OSs concentrations were $(41.1 \pm 34.5) \text{ ng/m}^3$ in Beijing, $(57.4 \pm 39.2) \text{ ng/m}^3$ in Taiyuan, and $(102.1 \pm 80.5) \text{ ng/m}^3$ in Changsha. Table S6 summarizes the average concentrations of $PM_{2.5}$, OC, gaseous pollutants, OS mass concentrations, and the mean meteorological parameters during sampling period for all three cities. OS accounted for $0.64\% \pm 0.44\%$, $0.41\% \pm 0.24\%$, and $0.76\% \pm 0.34\%$ of the total OA in Beijing, Taiyuan, and Changsha, respectively.



255 **Figure 1** Temporal variations of daily total OS mass concentrations and average OA mass
 256 concentrations in (a) Changsha, (b) Taiyuan, and (c) Beijing. The markers of OA mass concentrations
 257 are colored by average RH during sampling period, and marker sizes indicate the OS/OA mass
 258 concentration ratios.

260 The highest OS mass concentrations and OS/OA ratios were observed in Changsha. As shown in
 261 Figure 1(a), a distinct episode with OS mass concentrations exceeding 300 ng/m^3 occurred between
 262 December 27th and 31st, leading to the elevated OS mass concentrations in Changsha. This episode
 263 coincided with a period of intense fireworks activity, as evidenced by significant increases in the
 264 concentrations of recognized fireworks tracers, especially Ba and K (see Figure S4), leading to an
 265 increase in SO_2 emission. We noted that though K may originate from biomass burning, its trend in
 266 concentration shows good consistency with that of Ba. Therefore, we still infer that fireworks activity
 267 are also the primary source of K. Considering persistently high RH (consistently $>70\%$) during this
 268 period, as displayed in Figure S5, ALWC ($117.9 \mu\text{g/m}^3$ in average) therefore increased and facilitated
 269 the heterogeneous oxidation of SO_2 to particulate sulfate (Wang et al., 2016b; Ye et al., 2023). Since
 270 particulate sulfate serves as a key reactant in OS formation pathways, its elevated concentration
 271 directly promoted OS production (Xu et al., 2024; Wang et al., 2020). Furthermore, fireworks activity
 272 led to concurrent increases in the concentrations of transition metals, notably Fe and Mn (Figure S4),
 273 which are known to catalyze aqueous-phase radical chemistry and OS formation (Huang et al., 2019;
 274 Huang et al., 2018a). Therefore, the pronounced OS mass concentration during this period is attributed
 275 to a combination of elevated precursor emissions (SO_2), high-RH conditions favoring aqueous-phase
 276 processing, and the potential catalytic role of co-emitted transition metals.

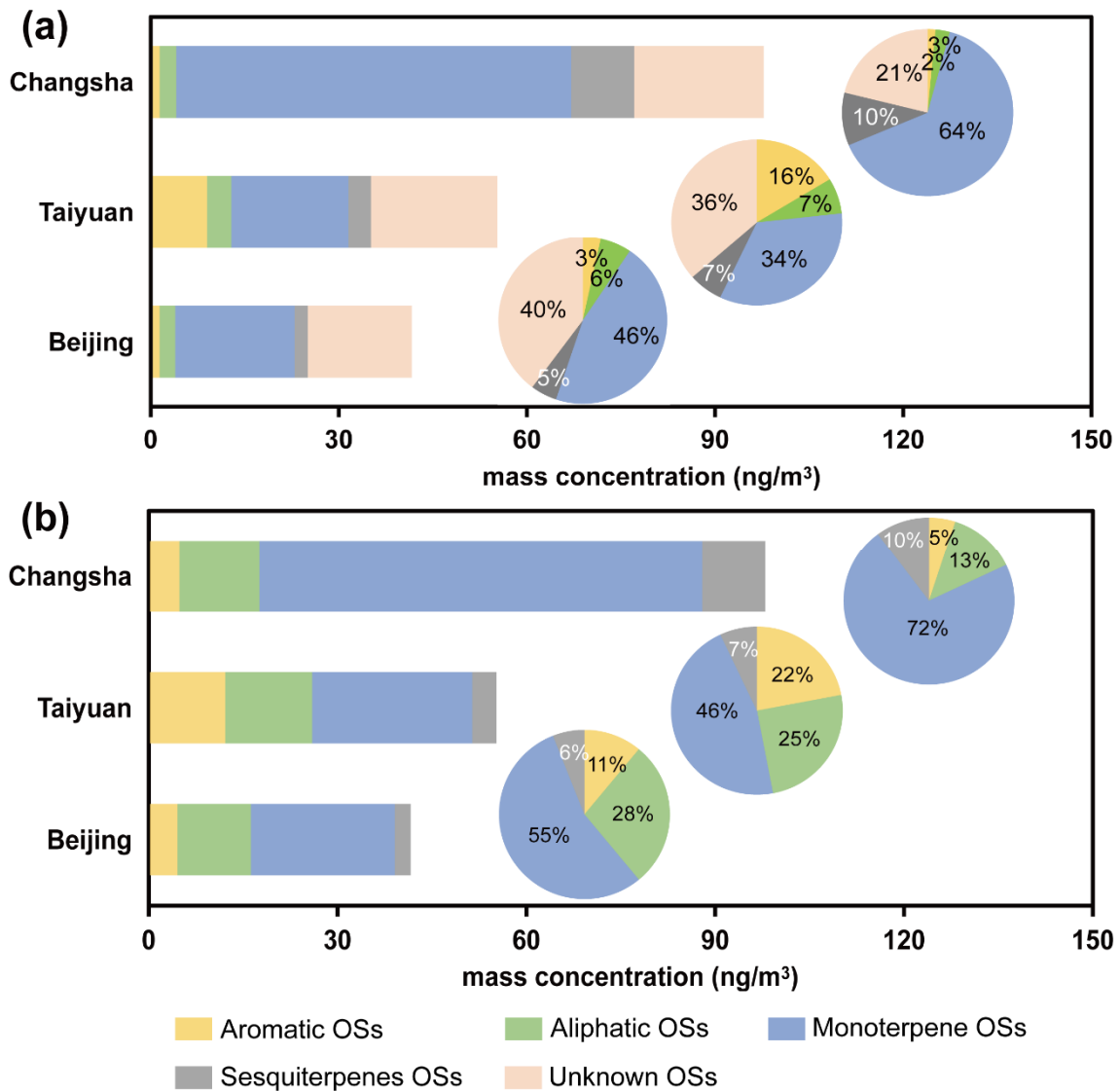
277 It is noteworthy that the single highest OS/OA ratio in Beijing was observed on December 31st
 278 under low RH. This phenomena highlights that ALWC, while a major driving factor of OS formation,

279 is not an exclusive control. Specifically, this day showed high atmospheric oxidative capacity and
280 aerosol acidity. We note that under such conditions, efficient acid-catalyzed heterogeneous reactions
281 of gas-phase oxidation products could drive substantial OS formation. The impact of ALWC,
282 atmospheric oxidative capacity, and aerosol pH on OS formation will be discussed in detail in Section
283 3.2.

284 Figures 2(a) and 2(b) shows the average mass concentrations and fractions of different OSs
285 categories across the three cities, based on classification approach based on OSs' elemental
286 composition and laboratory chamber-derived precursor–OS relationships and our precursor-based
287 PMF classification approach developed in this work, respectively (see Section 2.3 for details). As
288 displayed in Figure 2(b), Monoterpene OSs dominated detected OSs across all cities, contributing 55.2%
289 (Beijing), 46.8% (Taiyuan), and 72.3% (Changsha) to total OS, respectively. Biogenic-emitted
290 monoterpene is the precursor of Monoterpene OSs. However, monoterpene are primarily biogenic
291 precursors, their limited emissions during winter cannot fully explain the high mass fractions of
292 Monoterpene OSs. Recent studies have highlighted anthropogenic sources, particularly biomass
293 burning, as significant contributors to monoterpene (Wang et al., 2022a; Koss et al., 2018). The PM_{2.5}
294 source apportionment analysis (Text S2, Figure S6) confirmed that biomass burning substantially
295 contributed to PM_{2.5} across all cities. The highest total mass fractions of Monoterpene OSs in
296 Changsha are mainly attributed to the high RH (Table S6), which facilitates their formation via
297 heterogeneous reactions (Hettiyadura et al., 2017; Wang et al., 2018; Ding et al., 2016a; Ding et al.,
298 2016b; Li et al., 2020).

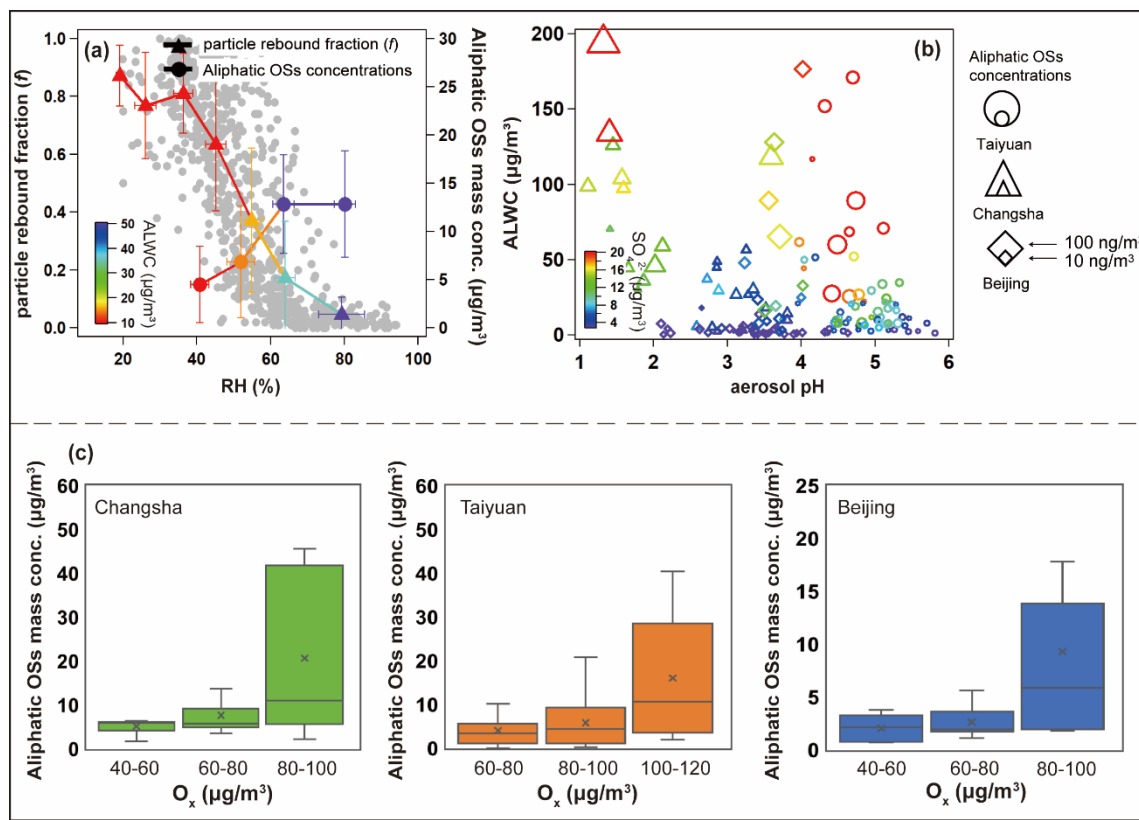
299 In Taiyuan, the total mass fractions of Aromatic OSs (21.2%) were significantly higher than those
300 in Beijing (10.7%) and Changsha (4.6%). Aromatic OSs primarily formed via aqueous-phase reactions
301 between S(IV) and aromatic VOCs (Huang et al., 2020). Taiyuan exhibited the highest sulfate mass
302 concentration among the three cities (Table S6), which promoted the formation of these species.
303 Additionally, transition metal ions—particularly Fe³⁺—catalyze aqueous-phase formation of Aromatic
304 OSs (Huang et al., 2020). High Fe mass concentration was observed in Taiyuan (0.79 ± 0.53 µg/m³),
305 further facilitated the formation of Aromatic OSs.

306 The highest total mass fractions of Aliphatic OSs were observed in Beijing (28.1%). Since vehicle
307 emissions, which is an important source of long-chain alkenes (He et al., 2022; Wang et al., 2021a;
308 Riva et al., 2016b; Tao et al., 2014; Tang et al., 2020), substantially contributed to PM_{2.5} in all cities
309 (Figure S6), the relative dominance of Aliphatic OSs in Beijing can be attributed to a comparative
310 reduction in the emissions of precursors for Monoterpene OSs and Aromatic OSs. Specifically, Beijing
311 exhibits lower emissions of monoterpene and aromatic VOCs precursors relative to Taiyuan and
312 Changsha, which results in a reduced contribution of Monoterpene and Aromatic OSs to the total OS
313 (see Figure 2(b)). Therefore, the relative mass fraction of Aliphatic OSs, which primarily derived from
314 between sulfate and photooxidation products of alkenes (Riva et al., 2016b), becomes more prominent
315 in Beijing. Additionally, low RH in Beijing further suppresses the aqueous-phase formation of
316 Monoterpene OSs, amplifying the relative importance of Aliphatic OSs.



332 60%) conditions.

333 In Changsha, where RH remains consistently high, Aliphatic OSs mass concentrations strongly
334 correlated with RH ($R = 0.78$). In Beijing and Taiyuan, correlations increased from low to medium
335 RH (Beijing: 0.53 to 0.82; Taiyuan: 0.38 to 0.77) but declined slightly at higher RH (Beijing: 0.82 to
336 0.69; Taiyuan: 0.77 to 0.72). The initial correlation rise reflects ALWC-enhanced sulfate-driven
337 heterogeneous OS formation (Wang et al., 2016a; Cheng et al., 2016), while the decline at elevated
338 RH may due to the increase in ALWC dilutes the concentrations of precursors and intermediates of
339 Aliphatic OSs within the aqueous phase. Therefore, Aliphatic OSs formation were not further
340 promoted, exhibiting the non-linear response of their mass concentrations and ALWC.



341

342 **Figure 3** (a) The measured particle rebound fraction (f) and total mass concentrations of Aliphatic OSs
343 as a function of RH, the plots were colored by the calculated ALWC concentrations in Taiyuan, grey
344 dots indicate the mass concentrations of Aliphatic OSs; (b) the relationship between aerosol pH and
345 ALWC across three cities, the markers were colored by the inorganic sulfate mass concentrations, the
346 marker sizes represented the total mass concentrations of Aliphatic OSs; (c) the box plot of total mass
347 concentrations of Aliphatic OSs at different O_x concentration levels.

348 This threshold behavior aligns with aerosol phase transitions. Particle rebound fraction (f),
349 indicating phase state, was measured in Taiyuan using a three-arm impactor (Liu et al., 2017). As RH
350 exceeded 60%, f dropped below 0.2 (Figure 3(a)), signaling a transition from non-liquid to liquid
351 aerosol states. This transition at $\text{RH} > 60\%$ aligns with prior field (Liu et al., 2017; Liu et al., 2023;
352 Meng et al., 2024; Song et al., 2022) and modeling (Qiu et al., 2023) studies in Eastern China.
353 Correspondingly, Aliphatic OSs concentrations increased with RH below 60% but plateaued beyond
354 that despite further humidity rises. These findings underscore aerosol phase state as a critical factor:

355 initial liquid phase formation (RH < 60%) promotes heterogeneous OS formation (Ye et al., 2018),
356 whereas at higher RH, saturation of reactive interfaces limits further ALWC effects.

357 In addition, the increase in ALWC with rising RH altered aerosol pH (Figure 3(b)), which
358 inhibited OSs formation via acid-catalyzed reactions (Duporté et al., 2016). In Changsha, as aerosol
359 pH increased from approximately 1.0 to above 3.0, the average total mass concentrations of Aliphatic
360 OSs decreased significantly from 9.3 to 4.6 ng/m³ (Figure S8), with further declines as pH increased.
361 In Taiyuan, OS concentrations dropped from 12.2 to 6.8 ng/m³ as pH rose from below 4.5 to above
362 5.0. However, in Beijing, total mass concentrations of Aliphatic OSs remained stable within a narrow
363 pH range of 3.2–3.9. Elevated ALWC facilitates aqueous-phase radical chemistry that forms OSs via
364 non-acid pathways, which can dominate over pH-dependent processes (Rudziński et al., 2009; Wach
365 et al., 2019; Huang et al., 2019). Thus, pH-dependent suppression of Aliphatic OSs formation is
366 common across urban aerosol pH ranges, but less evident when pH varies narrowly.

367 Inorganic sulfate plays a crucial role in OSs formation via sulfate esterification reactions (Xu et
368 al., 2024; Wang et al., 2020). We thus examined its effect on the formation of Aliphatic OSs. Figure
369 3(b) illustrates the relationships among ALWC, pH, inorganic sulfate mass concentration, and total
370 mass concentrations of Aliphatic OSs across all cities. A consistent positive correlation was observed,
371 consistent with previous field studies (Lin et al., 2022; Wang et al., 2023b; Le Breton et al., 2018;
372 Wang et al., 2018). This correlation was strongest when sulfate concentrations were below 20 µg/m³.
373 Below this threshold, total mass concentrations of Aliphatic OSs increased significantly with inorganic
374 sulfate, whereas above it, the correlation weakened. Additionally, inorganic sulfate mass concentration
375 showed a clear positive correlation with ALWC (Figure 3(b)), suggesting that ionic strength did not
376 increase linearly with sulfate mass. This likely reflects saturation effects in acid-mediated pathways,
377 driven by limitations in water activity and ionic strength (Wang et al., 2020). Overall, these results
378 highlight the nonlinear influence of inorganic sulfate on Aliphatic OSs formation.

379 Atmospheric oxidative capacity, represented by O_x (O_x = O₃ + NO₂) concentrations, typically
380 modulates OS formation via acid-catalyzed ring-opening reactions pathways. As shown in Figure 3(c),
381 total mass concentrations of Aliphatic OSs and NO_x OSs exhibited significant increases with rising O_x
382 levels across all cities. Especially, total mass concentrations of Aliphatic OSs significantly increased
383 across all cities when O_x concentrations raised from 60–80 µg/m³ to > 80 µg/m³. As shown in Figure
384 S9, O₃ dominated the O_x composition during high-O_x episodes (> 80 µg/m³) across all cities. Previous
385 laboratory studies have suggested that enhanced atmospheric oxidation capacities promote the
386 oxidation of VOCs (Zhang et al., 2022; Wei et al., 2024), forming cyclic intermediates. We therefore
387 inferred that the increase in O_x facilitates the formation of cyclic intermediates derived from long-
388 chain alkenes. Subsequent acid-catalyzed and ring-opening reactions are important pathways of
389 heterogeneous OSs formation, including Aliphatic OSs (Eddingsaas et al., 2010; Iinuma et al., 2007;
390 Brüggemann et al., 2020).

391 4 Conclusions and Implications

392 In this study, we applied a NTA approach based on UHPLC-HRMS to investigate the molecular
393 composition of OS in PM_{2.5} samples from three cities. By integrating molecular composition data,

394 precursor-constrained PMF source apportionment, and OS–precursor correlation analysis, we
395 developed a comprehensive method for accurate classification of detected OSs, demonstrating
396 superior discrimination between Aliphatic OSs. Conventional classification methods rely on
397 laboratory chamber-derived precursor–OS relationships (Wang et al., 2019a), which provide limited
398 insight into the formation of Aliphatic OSs and tend to underestimate their mass fractions. The
399 abundant Aliphatic OSs detected in ambient PM_{2.5} suggest complex formation pathways, such as OH
400 oxidation of long-chain alkenes (Riva et al., 2016b) and heterogeneous SO₂–alkene reactions in acidic
401 environments (Passananti et al., 2016), which remain incompletely understood in laboratory studies.
402 Our findings highlight the importance of emphasizing the formation of Aliphatic OSs in urban
403 atmospheres.

404 However, this study still faces several challenges. This work was conducted during the winter.
405 OS formation exhibits seasonal variability, particularly for pathways driven by biogenic VOCs
406 emissions and photochemical activity, which are generally enhanced in warmer months. Hence, the
407 underestimation of Aliphatic OSs, and their key formation factors determined in this work remain
408 valid insights for the winter period but may not fully represent annual OS behavior. Future long-term
409 observations are necessary to resolve the complete annual cycle of OS composition, quantify the
410 shifting contributions of anthropogenic versus biogenic precursors, and understanding how key
411 formation driving factors evolve with changing atmospheric conditions.

412 For NTA, the use of surrogate standards for quantification OS mass concentration introduced
413 uncertainty, particularly due to the extraction efficiency of individual OSs species from quartz fiber
414 filters could not be determined. Although we have adopted standardized extraction protocol ensures
415 high comparability across our samples, absolute extraction recoveries may vary. In addition, this
416 approach depends on public molecular composition such as mzCloud and ChemSpider integrated
417 within the Compound Discoverer software, which contain limited entries for organosulfates. Reliance
418 on these databases for compound identification may therefore underestimate OS mass concentrations
419 in urban environments. For example, OSs identified here accounted for less than 1% of total OA mass,
420 whereas recent work (Ma et al., 2025) reported approximately 20% contributions.

421 OS may become increasingly significant in OA, particularly in coastal regions influenced by
422 oceanic dimethyl sulfate emissions (Brüggemann et al., 2020). Our future work will focus on
423 synthesizing OSs standards representing various precursors and establishing a dedicated fragmentation
424 database through multi-platform MS² validation to elucidate OS sources in more detail.

425 **Author Contributions**

426 Y.Q., J.W., and Z.W. designed this work. J.L., Y.Wei, C.L., J.Y., T.L., R.M., T.Z., W.F., J.Y., Z.F., Y.X.
427 and K.B. collected PM_{2.5} samples. Y.Q., J.W., T.Q., Y.B., and D.L. conducted UHPLC-HRMS
428 experiments. Y.Q., J.W., Z.G., and Y.Wang wrote this manuscript. Z.W., Y.Wang, and M.H. edited this
429 manuscript. All authors have read and agreed to submit this manuscript. Y.Q. and J.W. contributed
430 equally to this work.

431 **Funding**

432 This work is funded by the National Nature Science Foundation of China (Grants 22221004 and
433 22306059). This work was also supported by the Science and Technology Innovation Program of

434 Hunan Province (Grants 2024RC3106 and 2025AQ2001), and the Fundamental Research Funds
435 for the Central Universities (Grant 531118010830).

436 **Notes**

437 The authors declare that they have no conflict of interest.

438 **Acknowledgements**

439 Y.W would like to acknowledge financial support by the National Nature Science Foundation of
440 China (Grants 22221004 and 22306059), This work was also supported by the Science and
441 Technology Innovation Program of Hunan Province (Grants 2024RC3106 and 2025AQ2001),
442 and the Fundamental Research Funds for the Central Universities (Grant 531118010830).

443

444 References

445 Bateman, A. P., Belassem, H., Martin, S. T.: Impactor Apparatus for the Study of Particle Rebound:
446 Relative Humidity and Capillary Forces. *Aerosol Science and Technology*. 48, 42-52.
447 10.1080/02786826.2013.853866, 2014.

448 Brüggemann, M., Xu, R., Tilgner, A., Kwong, K. C., Mutzel, A., Poon, H. Y., Otto, T., Schaefer, T.,
449 Poulain, L., Chan, M. N., Herrmann, H.: Organosulfates in Ambient Aerosol: State of Knowledge and
450 Future Research Directions on Formation, Abundance, Fate, and Importance. *Environmental Science &*
451 *Technology*. 54, 3767-3782. 10.1021/acs.est.9b06751, 2020.

452 Cai, D., Wang, X., Chen, J., Li, X.: Molecular Characterization of Organosulfates in Highly Polluted
453 Atmosphere Using Ultra-High-Resolution Mass Spectrometry. *Journal of Geophysical Research: Atmospheres*. 125, e2019JD032253. <https://doi.org/10.1029/2019JD032253>, 2020.

455 Cao, G., Zhao, X., Hu, D., Zhu, R., Ouyang, F.: Development and application of a quantification
456 method for water soluble organosulfates in atmospheric aerosols. *Environmental Pollution*. 225, 316-322.
457 <https://doi.org/10.1016/j.envpol.2017.01.086>, 2017.

458 Cheng, Y., Zheng, G., Wei, C., Mu, Q., Zheng, B., Wang, Z., Gao, M., Zhang, Q., He, K., Carmichael,
459 G., Pöschl, U., Su, H.: Reactive nitrogen chemistry in aerosol water as a source of sulfate during haze events
460 in China. 2, e1601530. doi:10.1126/sciadv.1601530, 2016.

461 Deng, Y., Inomata, S., Sato, K., Ramasamy, S., Morino, Y., Enami, S., Tanimoto, H.: Temperature and
462 acidity dependence of secondary organic aerosol formation from α -pinene ozonolysis with a compact
463 chamber system. *Atmos. Chem. Phys.* 21, 5983-6003. 10.5194/acp-21-5983-2021, 2021.

464 Ding, X., He, Q.-F., Shen, R.-Q., Yu, Q.-Q., Zhang, Y.-Q., Xin, J.-Y., Wen, T.-X., Wang, X.-M.: Spatial
465 and seasonal variations of isoprene secondary organic aerosol in China: Significant impact of biomass
466 burning during winter. *Scientific Reports*. 6, 20411. 10.1038/srep20411, 2016a.

467 Ding, X., Zhang, Y.-Q., He, Q.-F., Yu, Q.-Q., Shen, R.-Q., Zhang, Y., Zhang, Z., Lyu, S.-J., Hu, Q.-H.,
468 Wang, Y.-S., Li, L.-F., Song, W., Wang, X.-M.: Spatial and seasonal variations of secondary organic aerosol
469 from terpenoids over China. *Journal of Geophysical Research: Atmospheres*. 121, 14,661-614,678.
470 <https://doi.org/10.1002/2016JD025467>, 2016b.

471 Duporté, G., Flaud, P. M., Geneste, E., Augagneur, S., Pangui, E., Lamkaddam, H., Gratien, A.,
472 Doussin, J. F., Budzinski, H., Villenave, E., Perraquin, E.: Experimental Study of the Formation of
473 Organosulfates from α -Pinene Oxidation. Part I: Product Identification, Formation Mechanisms and Effect
474 of Relative Humidity. *The Journal of Physical Chemistry A*. 120, 7909-7923. 10.1021/acs.jpca.6b08504,
475 2016.

476 Duporté, G., Flaud, P. M., Kammer, J., Geneste, E., Augagneur, S., Pangui, E., Lamkaddam, H.,
477 Gratien, A., Doussin, J. F., Budzinski, H., Villenave, E., Perraquin, E.: Experimental Study of the Formation
478 of Organosulfates from α -Pinene Oxidation. 2. Time Evolution and Effect of Particle Acidity. *The Journal*
479 *of Physical Chemistry A*. 124, 409-421. 10.1021/acs.jpca.9b07156, 2020.

480 Eddingsaas, N. C., VanderVelde, D. G., Wennberg, P. O.: Kinetics and Products of the Acid-Catalyzed

481 Ring-Opening of Atmospherically Relevant Butyl Epoxy Alcohols. *The Journal of Physical Chemistry A.*
482 114, 8106-8113. 10.1021/jp103907c, 2010.

483 Estillore, A. D., Hettiyadura, A. P. S., Qin, Z., Leckrone, E., Wombacher, B., Humphry, T., Stone, E.
484 A., Grassian, V. H.: Water Uptake and Hygroscopic Growth of Organosulfate Aerosol. *Environmental*
485 *Science & Technology*. 50, 4259-4268. 10.1021/acs.est.5b05014, 2016.

486 Fleming, L. T., Ali, N. N., Blair, S. L., Roveretto, M., George, C., Nizkorodov, S. A.: Formation of
487 Light-Absorbing Organosulfates during Evaporation of Secondary Organic Material Extracts in the
488 Presence of Sulfuric Acid. *ACS Earth and Space Chemistry*. 3, 947-957.
489 10.1021/acsearthspacechem.9b00036, 2019.

490 Fountoukis, C., Nenes, A.: ISORROPIA II: a computationally efficient thermodynamic equilibrium
491 model for K⁺; Ca²⁺; Mg²⁺; NH⁴⁺; Na⁺; SO₄²⁻; NO₃⁻; Cl⁻; H₂O aerosols. *Atmospheric Chemistry and*
492 *Physics*. 7, 4639-4659. 10.5194/acp-7-4639-2007, 2007.

493 Guenther, A., Karl, T., Harley, P., Wiedinmyer, C., Palmer, P. I., Geron, C.: Estimates of global
494 terrestrial isoprene emissions using MEGAN (Model of Emissions of Gases and Aerosols from Nature).
495 *Atmos. Chem. Phys.* 6, 3181-3210. 10.5194/acp-6-3181-2006, 2006.

496 Hansen, A. M. K., Hong, J., Raatikainen, T., Kristensen, K., Ylisirniö, A., Virtanen, A., Petäjä, T.,
497 Glasius, M., Prisle, N. L.: Hygroscopic properties and cloud condensation nuclei activation of limonene-
498 derived organosulfates and their mixtures with ammonium sulfate. *Atmos. Chem. Phys.* 15, 14071-14089.
499 10.5194/acp-15-14071-2015, 2015.

500 He, J., Li, L., Li, Y., Huang, M., Zhu, Y., Deng, S.: Synthesis, MS/MS characteristics and quantification
501 of six aromatic organosulfates in atmospheric PM_{2.5}. *Atmospheric Environment*. 290, 119361.
502 <https://doi.org/10.1016/j.atmosenv.2022.119361>, 2022.

503 Hettiyadura, A. P. S., Jayarathne, T., Baumann, K., Goldstein, A. H., de Gouw, J. A., Koss, A., Keutsch,
504 F. N., Skog, K., Stone, E. A.: Qualitative and quantitative analysis of atmospheric organosulfates in
505 Centreville, Alabama. *Atmospheric Chemistry and Physics*. 17, 1343-1359. 10.5194/acp-17-1343-2017,
506 2017.

507 Hoyle, C. R., Boy, M., Donahue, N. M., Fry, J. L., Glasius, M., Guenther, A., Hallar, A. G., Huff Hartz,
508 Petters, M. D., Petäjä, T., Rosenoern, T., Sullivan, A. P.: A review of the anthropogenic influence on
509 biogenic secondary organic aerosol. *Atmos. Chem. Phys.* 11, 321-343. 10.5194/acp-11-321-2011, 2011.

510 Huang, L., Cochran, R. E., Coddens, E. M., Grassian, V. H.: Formation of Organosulfur Compounds
511 through Transition Metal Ion-Catalyzed Aqueous Phase Reactions. *Environmental Science & Technology*
512 Letters. 5, 315-321. 10.1021/acs.estlett.8b00225, 2018a.

513 Huang, L., Coddens, E. M., Grassian, V. H.: Formation of Organosulfur Compounds from Aqueous
514 Phase Reactions of S(IV) with Methacrolein and Methyl Vinyl Ketone in the Presence of Transition Metal
515 Ions. *ACS Earth and Space Chemistry*. 3, 1749-1755. 10.1021/acsearthspacechem.9b00173, 2019.

516 Huang, L., Liu, T., Grassian, V. H.: Radical-Initiated Formation of Aromatic Organosulfates and
517 Sulfonates in the Aqueous Phase. *Environmental Science & Technology*. 54, 11857-11864.
518 10.1021/acs.est.0c05644, 2020.

519 Huang, L., Wang, Y., Zhao, Y., Hu, H., Yang, Y., Wang, Y., Yu, J.-Z., Chen, T., Cheng, Z., Li, C., Li,
520 Z., Xiao, H.: Biogenic and Anthropogenic Contributions to Atmospheric Organosulfates in a Typical
521 Megacity in Eastern China. *Journal of Geophysical Research: Atmospheres*. 128, e2023JD038848.
522 <https://doi.org/10.1029/2023JD038848>, 2023a.

523 Huang, L., Wang, Y., Zhao, Y., Hu, H., Yang, Y., Wang, Y., Yu, J.-Z., Chen, T., Cheng, Z., Li, C., Li,
524 Z., Xiao, H.: Biogenic and Anthropogenic Contributions to Atmospheric Organosulfates in a Typical
525 Megacity in Eastern China. 128, e2023JD038848. <https://doi.org/10.1029/2023JD038848>, 2023b.

526 Huang, R. J., Cao, J., Chen, Y., Yang, L., Shen, J., You, Q., Wang, K., Lin, C., Xu, W., Gao, B., Li, Y.,
527 Chen, Q., Hoffmann, T., O'Dowd, C. D., Bilde, M., Glasius, M.: Organosulfates in atmospheric aerosol:
528 synthesis and quantitative analysis of PM2.5 from Xi'an, northwestern China. *Atmos. Meas. Tech.* 11, 3447-
529 3456. 10.5194/amt-11-3447-2018, 2018b.

530 Iinuma, Y., Müller, C., Berndt, T., Böge, O., Claeys, M., Herrmann, H.: Evidence for the Existence of
531 Organosulfates from β -Pinene Ozonolysis in Ambient Secondary Organic Aerosol. *Environmental Science
& Technology*. 41, 6678-6683. 10.1021/es070938t, 2007.

533 Jiang, H., Cai, J., Feng, X., Chen, Y., Guo, H., Mo, Y., Tang, J., Chen, T., Li, J., Zhang, G.:
534 Organosulfur Compounds: A Non-Negligible Component Affecting the Light Absorption of Brown Carbon
535 During North China Haze Events. *Journal of Geophysical Research: Atmospheres*. 130, e2024JD042043.
536 <https://doi.org/10.1029/2024JD042043>, 2025.

537 Koss, A. R., Sekimoto, K., Gilman, J. B., Selimovic, V., Coggon, M. M., Zarzana, K. J., Yuan, B.,
538 Lerner, B. M., Brown, S. S., Jimenez, J. L., Krechmer, J., Roberts, J. M., Warneke, C., Yokelson, R. J., de
539 Gouw, J.: Non-methane organic gas emissions from biomass burning: identification, quantification, and
540 emission factors from PTR-ToF during the FIREX 2016 laboratory experiment. *Atmos. Chem. Phys.* 18,
541 3299-3319. 10.5194/acp-18-3299-2018, 2018.

542 Le Breton, M., Wang, Y., Hallquist, Å. M., Pathak, R. K., Zheng, J., Yang, Y., Shang, D., Glasius, M.,
543 Bannan, T. J., Liu, Q., Chan, C. K., Percival, C. J., Zhu, W., Lou, S., Topping, D., Wang, Y., Yu, J., Lu, K.,
544 Guo, S., Hu, M., Hallquist, M.: Online gas- and particle-phase measurements of organosulfates,
545 organosulfonates and nitrooxy organosulfates in Beijing utilizing a FIGAERO ToF-CIMS. *Atmos. Chem.
546 Phys.* 18, 10355-10371. 10.5194/acp-18-10355-2018, 2018.

547 Li, L., Yang, W., Xie, S., Wu, Y.: Estimations and uncertainty of biogenic volatile organic compound
548 emission inventory in China for 2008–2018. *Science of The Total Environment*. 733, 139301.
549 <https://doi.org/10.1016/j.scitotenv.2020.139301>, 2020.

550 Lin, P., Yu, J. Z., Engling, G., Kalberer, M.: Organosulfates in Humic-like Substance Fraction Isolated
551 from Aerosols at Seven Locations in East Asia: A Study by Ultra-High-Resolution Mass Spectrometry.
552 *Environmental Science & Technology*. 46, 13118-13127. 10.1021/es303570v, 2012.

553 Lin, Y., Han, Y., Li, G., Wang, Q., Zhang, X., Li, Z., Li, L., Prévôt, A. S. H., Cao, J.: Molecular
554 Characteristics of Atmospheric Organosulfates During Summer and Winter Seasons in Two Cities of
555 Southern and Northern China. *Journal of Geophysical Research: Atmospheres*. 127, e2022JD036672.
556 <https://doi.org/10.1029/2022JD036672>, 2022.

557 Liu, P., Ding, X., Li, B. X., Zhang, Y. Q., Bryant, D. J., Wang, X. M.: Quality assurance and quality

558 control of atmospheric organosulfates measured using hydrophilic interaction liquid chromatography
559 (HILIC). *Atmos. Meas. Tech.* 17, 3067-3079. 10.5194/amt-17-3067-2024, 2024.

560 Liu, Y., Wu, Z., Wang, Y., Xiao, Y., Gu, F., Zheng, J., Tan, T., Shang, D., Wu, Y., Zeng, L., Hu, M.,
561 Bateman, A. P., Martin, S. T.: Submicrometer Particles Are in the Liquid State during Heavy Haze Episodes
562 in the Urban Atmosphere of Beijing, China. *Environ. Sci. Technol. Lett.* 4, 427-432.
563 10.1021/acs.estlett.7b00352, 2017.

564 Liu, Y. C., Wu, Z. J., Qiu, Y. T., Tian, P., Liu, Q., Chen, Y., Song, M., Hu, M.: Enhanced Nitrate Fraction:
565 Enabling Urban Aerosol Particles to Remain in a Liquid State at Reduced Relative Humidity. *Geophysical
566 Research Letters*. 50, e2023GL105505. <https://doi.org/10.1029/2023GL105505>, 2023.

567 Lukács, H., Gelencsér, A., Hoffer, A., Kiss, G., Horváth, K., Hartyáni, Z.: Quantitative assessment of
568 organosulfates in size-segregated rural fine aerosol. *Atmos. Chem. Phys.* 9, 231-238. 10.5194/acp-9-231-
569 2009, 2009.

570 Ma, J., Ungeheuer, F., Zheng, F., Du, W., Wang, Y., Cai, J., Zhou, Y., Yan, C., Liu, Y., Kulmala, M.,
571 Daellenbach, K. R., Vogel, A. L.: Nontarget Screening Exhibits a Seasonal Cycle of PM2.5 Organic Aerosol
572 Composition in Beijing. *Environmental Science & Technology*. 56, 7017-7028. 10.1021/acs.est.1c06905,
573 2022.

574 Ma, J., Reininger, N., Zhao, C., Döbler, D., Rüdiger, J., Qiu, Y., Ungeheuer, F., Simon, M., D'Angelo,
575 L., Breuninger, A., David, J., Bai, Y., Li, Y., Xue, Y., Li, L., Wang, Y., Hildmann, S., Hoffmann, T., Liu, B.,
576 Niu, H., Wu, Z., Vogel, A. L.: Unveiling a large fraction of hidden organosulfates in ambient organic aerosol.
577 *Nature Communications*. 16, 4098. 10.1038/s41467-025-59420-y, 2025.

578 Meng, X., Wu, Z., Chen, J., Qiu, Y., Zong, T., Song, M., Lee, J., Hu, M.: Particle phase state and
579 aerosol liquid water greatly impact secondary aerosol formation: insights into phase transition and its role
580 in haze events. *Atmospheric Chemistry and Physics*. 24, 2399-2414. 10.5194/acp-24-2399-2024, 2024.

581 Mutzel, A., Poulain, L., Berndt, T., Iinuma, Y., Rodigast, M., Böge, O., Richters, S., Spindler, G., Sipilä,
582 M., Jokinen, T., Kulmala, M., Herrmann, H.: Highly Oxidized Multifunctional Organic Compounds
583 Observed in Tropospheric Particles: A Field and Laboratory Study. *Environmental Science & Technology*.
584 49, 7754-7761. 10.1021/acs.est.5b00885, 2015.

585 Ohno, P. E., Wang, J., Mahrt, F., Varelas, J. G., Aruffo, E., Ye, J., Qin, Y., Kiland, K. J., Bertram, A.
586 K., Thomson, R. J., Martin, S. T.: Gas-Particle Uptake and Hygroscopic Growth by Organosulfate Particles.
587 *ACS Earth and Space Chemistry*. 6, 2481-2490. 10.1021/acsearthspacechem.2c00195, 2022.

588 Passananti, M., Kong, L., Shang, J., Dupart, Y., Perrier, S., Chen, J., Donaldson, D. J., George, C.:
589 Organosulfate Formation through the Heterogeneous Reaction of Sulfur Dioxide with Unsaturated Fatty
590 Acids and Long-Chain Alkenes. *Angewandte Chemie International Edition*. 55, 10336-10339.
591 <https://doi.org/10.1002/anie.201605266>, 2016.

592 Qiu, Y., Liu, Y., Wu, Z., Wang, F., Meng, X., Zhang, Z., Man, R., Huang, D., Wang, H., Gao, Y., Huang,
593 C., Hu, M.: Predicting Atmospheric Particle Phase State Using an Explainable Machine Learning Approach
594 Based on Particle Rebound Measurements. *Environmental Science & Technology*. 57, 15055-15064.
595 10.1021/acs.est.3c05284, 2023.

596 Riva, M., Tomaz, S., Cui, T., Lin, Y.-H., Perraudin, E., Gold, A., Stone, E. A., Villenave, E., Surratt, J.
597 D.: Evidence for an Unrecognized Secondary Anthropogenic Source of Organosulfates and Sulfonates:
598 Gas-Phase Oxidation of Polycyclic Aromatic Hydrocarbons in the Presence of Sulfate Aerosol.
599 Environmental Science & Technology. 49, 6654-6664. 10.1021/acs.est.5b00836, 2015.

600 Riva, M., Budisulistiorini, S. H., Zhang, Z., Gold, A., Surratt, J. D.: Chemical characterization of
601 secondary organic aerosol constituents from isoprene ozonolysis in the presence of acidic aerosol.
602 Atmospheric Environment. 130, 5-13. <https://doi.org/10.1016/j.atmosenv.2015.06.027>, 2016a.

603 Riva, M., Da Silva Barbosa, T., Lin, Y. H., Stone, E. A., Gold, A., Surratt, J. D.: Chemical
604 characterization of organosulfates in secondary organic aerosol derived from the photooxidation of alkanes.
605 Atmospheric Chemistry and Physics. 16, 11001-11018. 10.5194/acp-16-11001-2016, 2016b.

606 Riva, M., Da Silva Barbosa, T., Lin, Y. H., Stone, E. A., Gold, A., Surratt, J. D.: Chemical
607 characterization of organosulfates in secondary organic aerosol derived from the photooxidation of alkanes.
608 Atmos. Chem. Phys. 16, 11001-11018. 10.5194/acp-16-11001-2016, 2016c.

609 Riva, M., Chen, Y., Zhang, Y., Lei, Z., Olson, N. E., Boyer, H. C., Narayan, S., Yee, L. D., Green, H.
610 S., Cui, T., Zhang, Z., Baumann, K., Fort, M., Edgerton, E., Budisulistiorini, S. H., Rose, C. A., Ribeiro, I.
611 O., e Oliveira, R. L., dos Santos, E. O., Machado, C. M. D., Szopa, S., Zhao, Y., Alves, E. G., de Sá, S. S.,
612 Hu, W., Knipping, E. M., Shaw, S. L., Duvoisin Junior, S., de Souza, R. A. F., Palm, B. B., Jimenez, J.-L.,
613 Glasius, M., Goldstein, A. H., Pye, H. O. T., Gold, A., Turpin, B. J., Vizuete, W., Martin, S. T., Thornton, J.
614 A., Dutcher, C. S., Ault, A. P., Surratt, J. D.: Increasing Isoprene Epoxydiol-to-Inorganic Sulfate Aerosol
615 Ratio Results in Extensive Conversion of Inorganic Sulfate to Organosulfur Forms: Implications for
616 Aerosol Physicochemical Properties. Environmental Science & Technology. 53, 8682-8694.
617 10.1021/acs.est.9b01019, 2019.

618 Rudziński, K. J., Gmachowski, L., Kuznetsova, I.: Reactions of isoprene and sulphonyl radical-anions
619 – a possible source of atmospheric organosulphites and organosulphates. Atmos. Chem. Phys. 9, 2129-2140.
620 10.5194/acp-9-2129-2009, 2009.

621 Sakulyanontvittaya, T., Guenther, A., Helmig, D., Milford, J., Wiedinmyer, C.: Secondary Organic
622 Aerosol from Sesquiterpene and Monoterpene Emissions in the United States. Environmental Science &
623 Technology. 42, 8784-8790. 10.1021/es800817r, 2008.

624 Song, M., Jeong, R., Kim, D., Qiu, Y., Meng, X., Wu, Z., Zuend, A., Ha, Y., Kim, C., Kim, H., Gaikwad,
625 S., Jang, K. S., Lee, J. Y., Ahn, J.: Comparison of Phase States of PM2.5 over Megacities, Seoul and Beijing,
626 and Their Implications on Particle Size Distribution. Environmental Science and Technology. 56, 17581-
627 17590. 10.1021/acs.est.2c06377, 2022.

628 Staudt, S., Kundu, S., Lehmler, H.-J., He, X., Cui, T., Lin, Y.-H., Kristensen, K., Glasius, M., Zhang,
629 X., Weber, R. J., Surratt, J. D., Stone, E. A.: Aromatic organosulfates in atmospheric aerosols: Synthesis,
630 characterization, and abundance. Atmospheric Environment. 94, 366-373.
631 <https://doi.org/10.1016/j.atmosenv.2014.05.049>, 2014.

632 Surratt, J. D., Gómez-González, Y., Chan, A. W. H., Vermeylen, R., Shahgholi, M., Kleindienst, T. E.,
633 Edney, E. O., Offenberg, J. H., Lewandowski, M., Jaoui, M., Maenhaut, W., Claeys, M., Flagan, R. C.,
634 Seinfeld, J. H.: Organosulfate Formation in Biogenic Secondary Organic Aerosol. The Journal of Physical

635 Chemistry A. 112, 8345-8378. 10.1021/jp802310p, 2008.

636 Tang, J., Li, J., Su, T., Han, Y., Mo, Y., Jiang, H., Cui, M., Jiang, B., Chen, Y., Tang, J., Song, J., Peng,
637 P., Zhang, G.: Molecular compositions and optical properties of dissolved brown carbon in biomass burning,
638 coal combustion, and vehicle emission aerosols illuminated by excitation–emission matrix spectroscopy
639 and Fourier transform ion cyclotron resonance mass spectrometry analysis. Atmos. Chem. Phys. 20, 2513-
640 2532. 10.5194/acp-20-2513-2020, 2020.

641 Tao, S., Lu, X., Levac, N., Bateman, A. P., Nguyen, T. B., Bones, D. L., Nizkorodov, S. A., Laskin, J.,
642 Laskin, A., Yang, X.: Molecular Characterization of Organosulfates in Organic Aerosols from Shanghai and
643 Los Angeles Urban Areas by Nanospray-Desorption Electrospray Ionization High-Resolution Mass
644 Spectrometry. Environmental Science & Technology. 48, 10993-11001. 10.1021/es5024674, 2014.

645 Tolocka, M. P., Turpin, B.: Contribution of Organosulfur Compounds to Organic Aerosol Mass.
646 Environmental Science & Technology. 46, 7978-7983. 10.1021/es300651v, 2012.

647 Wach, P., Spólnik, G., Rudziński, K. J., Skotak, K., Claeys, M., Danikiewicz, W., Szmigielski, R.:
648 Radical oxidation of methyl vinyl ketone and methacrolein in aqueous droplets: Characterization of
649 organosulfates and atmospheric implications. Chemosphere. 214, 1-9.
650 <https://doi.org/10.1016/j.chemosphere.2018.09.026>, 2019.

651 Wang, G., Zhang, R., Gomez, M. E., Yang, L., Levy Zamora, M., Hu, M., Lin, Y., Peng, J., Guo, S.,
652 Meng, J., Li, J., Cheng, C., Hu, T., Ren, Y., Wang, Y., Gao, J., Cao, J., An, Z., Zhou, W., Li, G., Wang, J.,
653 Tian, P., Marrero-Ortiz, W., Secrest, J., Du, Z., Zheng, J., Shang, D., Zeng, L., Shao, M., Wang, W., Huang,
654 Y., Wang, Y., Zhu, Y., Li, Y., Hu, J., Pan, B., Cai, L., Cheng, Y., Ji, Y., Zhang, F., Rosenfeld, D., Liss, P. S.,
655 Duce, R. A., Kolb, C. E., Molina, M. J.: Persistent sulfate formation from London Fog to Chinese haze.
656 113, 13630-13635. doi:10.1073/pnas.1616540113, 2016a.

657 Wang, G., Zhang, R., Gomez, M. E., Yang, L., Levy Zamora, M., Hu, M., Lin, Y., Peng, J., Guo, S.,
658 Meng, J., Li, J., Cheng, C., Hu, T., Ren, Y., Wang, Y., Gao, J., Cao, J., An, Z., Zhou, W., Li, G., Wang, J.,
659 Tian, P., Marrero-Ortiz, W., Secrest, J., Du, Z., Zheng, J., Shang, D., Zeng, L., Shao, M., Wang, W., Huang,
660 Y., Wang, Y., Zhu, Y., Li, Y., Hu, J., Pan, B., Cai, L., Cheng, Y., Ji, Y., Zhang, F., Rosenfeld, D., Liss, P. S.,
661 Duce, R. A., Kolb, C. E., Molina, M. J.: Persistent sulfate formation from London Fog to Chinese haze.
662 Proceedings of the National Academy of Sciences. 113, 13630-13635. 10.1073/pnas.1616540113, 2016b.

663 Wang, H., Ma, X., Tan, Z., Wang, H., Chen, X., Chen, S., Gao, Y., Liu, Y., Liu, Y., Yang, X., Yuan, B.,
664 Zeng, L., Huang, C., Lu, K., Zhang, Y.: Anthropogenic monoterpenes aggravating ozone pollution. National
665 Science Review. 9, nwac103. 10.1093/nsr/nwac103, 2022a.

666 Wang, K., Zhang, Y., Huang, R.-J., Wang, M., Ni, H., Kampf, C. J., Cheng, Y., Bilde, M., Glasius, M.,
667 Hoffmann, T.: Molecular Characterization and Source Identification of Atmospheric Particulate
668 Organosulfates Using Ultrahigh Resolution Mass Spectrometry. Environmental Science & Technology. 53,
669 6192-6202. 10.1021/acs.est.9b02628, 2019a.

670 Wang, Y., Ren, J., Huang, X. H. H., Tong, R., Yu, J. Z.: Synthesis of Four Monoterpene-Derived
671 Organosulfates and Their Quantification in Atmospheric Aerosol Samples. Environmental Science &
672 Technology. 51, 6791-6801. 10.1021/acs.est.7b01179, 2017.

673 Wang, Y., Hu, M., Guo, S., Wang, Y., Zheng, J., Yang, Y., Zhu, W., Tang, R., Li, X., Liu, Y., Le Breton,

674 M., Du, Z., Shang, D., Wu, Y., Wu, Z., Song, Y., Lou, S., Hallquist, M., Yu, J.: The secondary formation of
675 organosulfates under interactions between biogenic emissions and anthropogenic pollutants in summer in
676 Beijing. *Atmospheric Chemistry and Physics*. 18, 10693-10713. 10.5194/acp-18-10693-2018, 2018.

677 Wang, Y., Ma, Y., Li, X., Kuang, B. Y., Huang, C., Tong, R., Yu, J. Z.: Monoterpene and Sesquiterpene
678 α -Hydroxy Organosulfates: Synthesis, MS/MS Characteristics, and Ambient Presence. *Environmental*
679 *Science & Technology*. 53, 12278-12290. 10.1021/acs.est.9b04703, 2019b.

680 Wang, Y., Hu, M., Wang, Y.-C., Li, X., Fang, X., Tang, R., Lu, S., Wu, Y., Guo, S., Wu, Z., Hallquist,
681 M., Yu, J. Z.: Comparative Study of Particulate Organosulfates in Contrasting Atmospheric Environments:
682 Field Evidence for the Significant Influence of Anthropogenic Sulfate and NOx. *Environmental Science &*
683 *Technology Letters*. 7, 787-794. 10.1021/acs.estlett.0c00550, 2020.

684 Wang, Y., Zhao, Y., Wang, Y., Yu, J. Z., Shao, J., Liu, P., Zhu, W., Cheng, Z., Li, Z., Yan, N., Xiao, H.:
685 Organosulfates in atmospheric aerosols in Shanghai, China: seasonal and interannual variability, origin, and
686 formation mechanisms. *Atmos. Chem. Phys.* 21, 2959-2980. 10.5194/acp-21-2959-2021, 2021a.

687 Wang, Y., Zhao, Y., Wang, Y., Yu, J. Z., Shao, J., Liu, P., Zhu, W., Cheng, Z., Li, Z., Yan, N., Xiao, H.:
688 Organosulfates in atmospheric aerosols in Shanghai, China: seasonal and interannual variability, origin, and
689 formation mechanisms. *Atmospheric Chemistry and Physics*. 21, 2959-2980. 10.5194/acp-21-2959-2021,
690 2021b.

691 Wang, Y., Ma, Y., Kuang, B., Lin, P., Liang, Y., Huang, C., Yu, J. Z.: Abundance of organosulfates
692 derived from biogenic volatile organic compounds: Seasonal and spatial contrasts at four sites in China.
693 *Science of The Total Environment*. 806, 151275. <https://doi.org/10.1016/j.scitotenv.2021.151275>, 2022b.

694 Wang, Y., Feng, Z., Yuan, Q., Shang, D., Fang, Y., Guo, S., Wu, Z., Zhang, C., Gao, Y., Yao, X., Gao,
695 H., Hu, M.: Environmental factors driving the formation of water-soluble organic aerosols: A comparative
696 study under contrasting atmospheric conditions. *Science of The Total Environment*. 866, 161364.
697 <https://doi.org/10.1016/j.scitotenv.2022.161364>, 2023a.

698 Wang, Y., Liang, S., Le Breton, M., Wang, Q. Q., Liu, Q., Ho, C. H., Kuang, B. Y., Wu, C., Hallquist,
699 M., Tong, R., Yu, J. Z.: Field observations of C2 and C3 organosulfates and insights into their formation
700 mechanisms at a suburban site in Hong Kong. *Science of The Total Environment*. 904, 166851.
701 <https://doi.org/10.1016/j.scitotenv.2023.166851>, 2023b.

702 Wei, L., Liu, R., Liao, C., Ouyang, S., Wu, Y., Jiang, B., Chen, D., Zhang, T., Guo, Y., Liu, S. C.: An
703 observation-based analysis of atmospheric oxidation capacity in Guangdong, China. *Atmospheric*
704 *Environment*. 318, 120260. <https://doi.org/10.1016/j.atmosenv.2023.120260>, 2024.

705 Xu, L., Tsona, N. T., Du, L.: Relative Humidity Changes the Role of SO₂ in Biogenic Secondary
706 Organic Aerosol Formation. *The Journal of Physical Chemistry Letters*. 12, 7365-7372.
707 10.1021/acs.jpclett.1c01550, 2021a.

708 Xu, L., Yang, Z., Tsona, N. T., Wang, X., George, C., Du, L.: Anthropogenic–Biogenic Interactions at
709 Night: Enhanced Formation of Secondary Aerosols and Particulate Nitrogen- and Sulfur-Containing
710 Organics from β -Pinene Oxidation. *Environmental Science & Technology*. 55, 7794-7807.
711 10.1021/acs.est.0c07879, 2021b.

712 Xu, R., Chen, Y., Ng, S. I. M., Zhang, Z., Gold, A., Turpin, B. J., Ault, A. P., Surratt, J. D., Chan, M.
713 N.: Formation of Inorganic Sulfate and Volatile Nonsulfated Products from Heterogeneous Hydroxyl
714 Radical Oxidation of 2-Methyltetrol Sulfate Aerosols: Mechanisms and Atmospheric Implications.
715 Environmental Science & Technology Letters. 11, 968-974. 10.1021/acs.estlett.4c00451, 2024.

716 Yang, T., Xu, Y., Ye, Q., Ma, Y. J., Wang, Y. C., Yu, J. Z., Duan, Y. S., Li, C. X., Xiao, H. W., Li, Z. Y.,
717 Zhao, Y., Xiao, H. Y.: Spatial and diurnal variations of aerosol organosulfates in summertime Shanghai,
718 China: potential influence of photochemical processes and anthropogenic sulfate pollution. Atmos. Chem.
719 Phys. 23, 13433-13450. 10.5194/acp-23-13433-2023, 2023.

720 Yang, T., Xu, Y., Ma, Y.-J., Wang, Y.-C., Yu, J. Z., Sun, Q.-B., Xiao, H.-W., Xiao, H.-Y., Liu, C.-Q.:
721 Field Evidence for Constraints of Nearly Dry and Weakly Acidic Aerosol Conditions on the Formation of
722 Organosulfates. Environmental Science & Technology Letters. 11, 981-987. 10.1021/acs.estlett.4c00522,
723 2024.

724 Yassine, M. M., Harir, M., Dabek-Zlotorzynska, E., Schmitt-Kopplin, P.: Structural characterization
725 of organic aerosol using Fourier transform ion cyclotron resonance mass spectrometry: Aromaticity
726 equivalent approach. Rapid Communications in Mass Spectrometry. 28, 2445-2454.
727 <https://doi.org/10.1002/rcm.7038>, 2014.

728 Ye, C., Lu, K., Song, H., Mu, Y., Chen, J., Zhang, Y.: A critical review of sulfate aerosol formation
729 mechanisms during winter polluted periods. Journal of Environmental Sciences. 123, 387-399.
730 <https://doi.org/10.1016/j.jes.2022.07.011>, 2023.

731 Ye, J., Abbatt, J. P. D., Chan, A. W. H.: Novel pathway of SO₂ oxidation in the atmosphere: reactions
732 with monoterpene ozonolysis intermediates and secondary organic aerosol. Atmos. Chem. Phys. 18, 5549-
733 5565. 10.5194/acp-18-5549-2018, 2018.

734 Zhang, Y., Chen, Y., Lei, Z., Olson, N. E., Riva, M., Koss, A. R., Zhang, Z., Gold, A., Jayne, J. T.,
735 Worsnop, D. R., Onasch, T. B., Kroll, J. H., Turpin, B. J., Ault, A. P., Surratt, J. D.: Joint Impacts of Acidity
736 and Viscosity on the Formation of Secondary Organic Aerosol from Isoprene Epoxydiols (IEPOX) in Phase
737 Separated Particles. ACS Earth and Space Chemistry. 3, 2646-2658. 10.1021/acsearthspacechem.9b00209,
738 2019.

739 Zhang, Z., Jiang, J., Lu, B., Meng, X., Herrmann, H., Chen, J., Li, X.: Attributing Increases in Ozone
740 to Accelerated Oxidation of Volatile Organic Compounds at Reduced Nitrogen Oxides Concentrations.
741 PNAS Nexus. 1, pgac266. 10.1093/pnasnexus/pgac266, 2022.

742 Zhao, D., Schmitt, S. H., Wang, M., Acir, I. H., Tillmann, R., Tan, Z., Novelli, A., Fuchs, H., Pullinen,
743 I., Wegener, R., Rohrer, F., Wildt, J., Kiendler-Scharr, A., Wahner, A., Mentel, T. F.: Effects of NO_x and
744 SO₂ on the secondary organic aerosol formation from photooxidation of α -pinene and limonene. Atmos.
745 Chem. Phys. 18, 1611-1628. 10.5194/acp-18-1611-2018, 2018.

746